Biomaterials 248 (2020) 120014

Contents lists available at ScienceDirect

Biomaterials

journal homepage: www.elsevier.com/locate/biomaterials

Decoupling the effects of nanopore size and surface roughness on the attachment, spreading and differentiation of bone marrow-derived stem cells

Jing Xia[a], Yuan Yuan[a], Huayin Wu[a], Yuting Huang[a], David A. Weitz[a,b,*]

[a] School of Engineering and Applied Sciences, Harvard University, Cambridge, MA, 02138, USA
[b] Department of Physics, Harvard University, Cambridge, MA, 02138, USA

ARTICLE INFO

Keywords:
Mesenchymal stem cell
Nanopore size
Roughness
Two-dimensional nanoporous surface
Cell morphology
Osteogenic differentiation

ABSTRACT

The nanopore size and roughness of nanoporous surface are two critical variables in determining stem cell fate, but little is known about the contribution from each cue individually. To address this gap, we use two-dimensional nanoporous membranes with controlled nanopore size and roughness to culture bone marrow-derived mesenchymal stem cells (BMSCs), and study their behaviors such as attachment, spreading and differentiation. We find that increasing the roughness of nanoporous surface has no noticeable effect on cell attachment, and only slightly decreases cell spreading areas and inhibits osteogenic differentiation. However, BMSCs cultured on membranes with larger nanopores have significantly fewer attached cells and larger spreading areas. Moreover, these cells cultured on larger nanopores undergo enhanced osteogenic differentiation by expressing more alkaline phosphatase, osteocalcin, osteopontin, and secreting more collagen type I. These results suggest that although both nanopore size and roughness can affect BMSCs, nanopore size plays a more significant role than roughness in controlling BMSC behavior.

1. Introduction

Bone marrow-derived mesenchymal stem cells (BMSC) are skeletal progenitor cells that originate from bone marrow, which has the ability to differentiate into many cell types such as adipocyte cell, osteoblast cell and chondrocyte cell[1,2]. Among all three differentiation lineages, osteogenic cells, which are responsible for the bone remodeling and regeneration [3,4], have long been regarded as a potential cellular substrate to cure bone diseases such as osteoporosis, or repair bone tissues by growing new bone around artificial implant [5–9]. By designing the two-dimensional surface topography of bone implant on the nanometer scale, growth of BMSCs around implant can be promoted and thus enable enhanced bone healing [10–12]. In particular, since nanoporous surface topography of bone plays a key role in guiding bone tissue formation, mimicking this nanoporous surface topography to design artificial implant is thought to direct the fate of BMSCs similar to native bone structure, which can promote better clinical performance [13–16].

Nanoporous surface topography can be characterized by many parameters, with nanopore size and surface roughness being two of the most fundamental ones. Both parameters can dramatically affect the behavior of BMSC cells such as attachment, spreading and differentiation, which are all critical to cell survival and function[17–19]. By mimicking the nanopore of bones, nanotube of pore size between 15 and 100 nm has shown significant influence on the differentiation lineage of BMSCs [15,16,20]. In addition, by culturing cells on non-porous surface with similar roughness to cortical bone (10–100 nm) [21], it was shown that roughness has no significant influence on cell differentiation, but the rough surface can improve BMSC cell adhesion compared with smooth surface [22]. However, a significant limitation of current studies is that these two factors are often coupled due to the material fabrication processes, which makes it unclear to which extent does each factor contribute to BMSC behavior. Therefore, to better design bone implant surface using nanoporous topography that can precisely regulate BMSC cell behavior, it is necessary to decouple the contribution of nanopore size and roughness.

In this paper, the goal is to distinguish the contribution of nanopore size and roughness to the BMSCs behavior. To achieve this, we culture BMSCs on biocompatible nanoporous polycarbonate membranes with controlled nanopore size and surface roughness, yet with similar stiffness to cortical bones [23]. One side of the membrane is much rougher than the other, while the nanopore size is the same. Thus, by comparing

* Corresponding author. School of Engineering and Applied Sciences, Harvard University, Cambridge, MA, 02138, USA.
E-mail address: weitz@seas.harvard.edu (D.A. Weitz).

https://doi.org/10.1016/j.biomaterials.2020.120014
Received 29 August 2019; Received in revised form 24 March 2020; Accepted 27 March 2020
Available online 31 March 2020

the behavior of cells on either side, and by using membranes with different nanopore size, we can distinguish the effects of nanopore size and roughness on cell behavior. Our results show that increasing the roughness of nanoporous surface has no obvious effect on cell attachment, and only slightly decrease cell spreading area and inhibit osteogenic differentiation. In addition, BMSCs cultured on membranes with larger nanopores have significantly fewer attached cells and larger spreading area. Moreover, cells undergo enhanced osteogenic differentiation by expressing more alkaline phosphatase, osteocalcin, osteopontin, and secreting more collagen type I. Our results suggest that, compared with surface roughness, nanopore size plays a more significant role in governing BMSC cell behavior: larger nanopore can significantly enhance cell spreading and osteogenic differentiation.

2. Materials and methods

2.1. Nanoporous membranes characterization

Surface topography of membranes is characterized by Cypher Atomic Force Microscope (Oxford Instruments Asylum Research, Inc., CA, USA). A cantilever with a cone tip (Innovative Solutions Bulgaria Ltd., Sofia, Bulgaria) is used to scan a 30 μm * 30 μm area in the air-tapping mode. The arithmetic average roughness of the solid regions excluding the nanopores of the membranes are measured by Igor pro software (WaveMetrics, OR, USA). To visualize the nanopore distribution on membranes, scanning electron microscopy images are taken with Ultra55 scanning electron microscope (Carl Zeiss Microscopy, LLC, NY, USA). Nanopore size and density are quantified by ImageJ (https://imagej.nih.gov/ij/). For characterization of the membrane surface chemistry, X-ray photoelectron spectrometer (XPS) analysis is performed with a K-Alpha XPS System (Thermal Fisher Scientific, Waltham, MA) to scan the membranes from 0eV to 1350 eV with 1 eV step size.

2.2. Cell culture membranes fabrication

To fabricate the cell culture membrane assembly, hydrophilic polycarbonate membranes (Sterlitech Corporation, WA, USA) of different nanopore sizes (10 nm, 80 nm, 200 nm) are sandwiched between stainless steel metal washers (Mcmaster, NJ, USA) and laser cut ring made with 0.004″ polyester shim stock (Mcmaster, NJ, USA). This sandwich assembly is glued between each layer using epoxy NOA81 (Norland Product Inc, NJ, USA) and cured under a 365 nm wavelength handheld UV lamp (AnalytikJena, Germany) for 1 h. Each side of the cell culture membrane assembly is sterilized with a germicidal lamp in the biosafety cabinet for 40 min. Cell culture membrane assemblies are subsequently transferred to a 35 mm glass-bottom Petri dish (Cellvis, CA, USA) and immersed in PBS for 2 h before cell seeding.

2.3. Cell culture

Human bone marrow-derived mesenchymal stem cells (hBMSCs) (ATCC, VA, USA) are used in this study. MSC growth medium is prepared by mixing mesenchymal stem cell basal medium (ATCC, VA, USA) with mesenchymal stem cell growth kit (ATCC, VA, USA). Cells are cultured in the MSC growth medium and maintained in the 37 °C, 5% CO2 infused incubator. All experiments are carried out with early passage hBMSCs (passage 2–passage 6).

2.4. Cell attachment and morphology assay

For cell morphological (Area, Volume, Height) and attachment studies, cells are stained with the celltracker green CMFDA dye (Thermo Fisher Scientific Inc, MA, USA) before seeding. Briefly, cells are centrifuged at 400 g-force after trypsinization, and re-suspended in the staining medium (2 μg/ml celltracker green CMFDA in MSC growth medium). After 40 min, stained cells are centrifuged again at 400 g-force to remove the staining medium and re-suspended in the MSC growth medium. Stained cells are then seeded onto the cell culture membrane assemblies at a density around 5000 cells/cm^2, and are subsequently cultured in the 37 °C, 5% CO2 infused incubator. After 16 h, cells are fixed with 4% formaldehyde (Sigma-Aldrich, MO, USA) and 0.1% Triton X-100 (Sigma-Aldrich, MO, USA) diluted in PBS (Sigma-Aldrich, MO, USA), followed by PBS wash for 3 times to remove excessive reagents. After cell fixation, DAPI (Sigma-Aldrich, MO, USA) is used to stain cell nucleus at a final concentration of 1 μg/ml for 20 min. Stained cells are then washed 3 times for 5 min each with PBS and imaged with the confocal microscope (see Optical microscopic imaging).

2.5. Cell focal adhesion immunofluorescence assay

For observation of the cell focal adhesions, cells are seeded onto cell culture membrane assemblies at a density around 5000 cells/cm^2, and cultured in the 37 °C, 5% CO2 infused incubator for 16 h. Cells are fixed with 4% formaldehyde and 0.1% Triton X100 diluted in PBS, followed by PBS wash for 3 times to remove excessive reagents. After cell fixation, cells are triple stained for actin, vinculin, and nucleus. Fixed cells are blocked with 10% bovine serum albumin (Thermo Fisher Scientific Inc, MA, USA) in PBS for 1 h, followed by a two-step immunostaining process for vinculin. Briefly, cells are first incubated with mouse monoclonal *anti*-vinculin antibody (Sigma-Aldrich, MO, USA) diluted 200X in PBS with a supplement of 10% normal goat serum for 1 h at room temperature. Samples are then washed 5 times for 5 min each with PBS and incubated with goat anti-mouse alexa fluor plus 488 secondary antibodies diluted 200X in PBS with a supplement of 10% Normal goat serum for 1 h in the dark. To stain actin and nucleus, Phalloidin-iFluor 555 (Abcam, MA, USA) and Draq 5 nucleus probe (Thermo Fisher Scientific Inc, MA, USA) are diluted at 1:1000 and 1:5000 each to incubate cells for 1 h. Stained cells are then washed 3 times for 5 min each with PBS and imaged with the confocal microscope (see Optical microscopic imaging).

2.6. Cell osteogenic differentiation assay

For cell differentiation study, cells are seeded on cell culture membrane assemblies at a density around 8000 cells/cm^2 and cultured in MSC growth medium overnight. Cell culture membrane assemblies are then transferred to a new Petri dish to keep only the cells attached on membranes. Cells are cultured in MSC growth media for 5–7 days until reaching confluency. Then the culture medium is switched to the osteogenic differentiation medium for osteogenic differentiation. Osteogenic differentiation medium is prepared by mixing human osteogenic supplement (R&D Systems, Inc., MN, USA) with stemXVivo osteogenic/adipogenic base media (R&D Systems, Inc., MN, USA). Cell are cultured with fresh osteogenic differentiation medium changed every three days.

For staining of alkaline phosphatase protein and collagen type I, cells are fixed after 16–18 days of culture in osteogenic differentiation medium. Briefly, cells are fixed with 4% formaldehyde and 0.1% Triton X100 diluted in PBS, followed by PBS wash for 3 times to remove excessive reagents. After fixation, cells are triple stained for alkaline phosphatase protein, collagen type I, and nucleus. ImmPACT Vector Red Alkaline Phosphatase Substrate (Vector Laboratories, CA, USA) is used to stain alkaline phosphatase protein. Briefly, reagent 1 and 2 from the kit is mixed with Vector Red Diluent and incubate with fixed cells for 1 h in the dark, followed by PBS wash for three times. To stain collagen type I, fixed cells are blocked with 10% normal goat serum (Thermo Fisher Scientific Inc, MA, USA) in PBS for 1 h, followed by a two-step immunostaining process. Briefly, fixed cells are incubated with COL1A mouse monoclonal antibody (Santa Cruz Biotechnology, TX, USA) diluted 200 times in 10% normal goat serum for 1 h at room

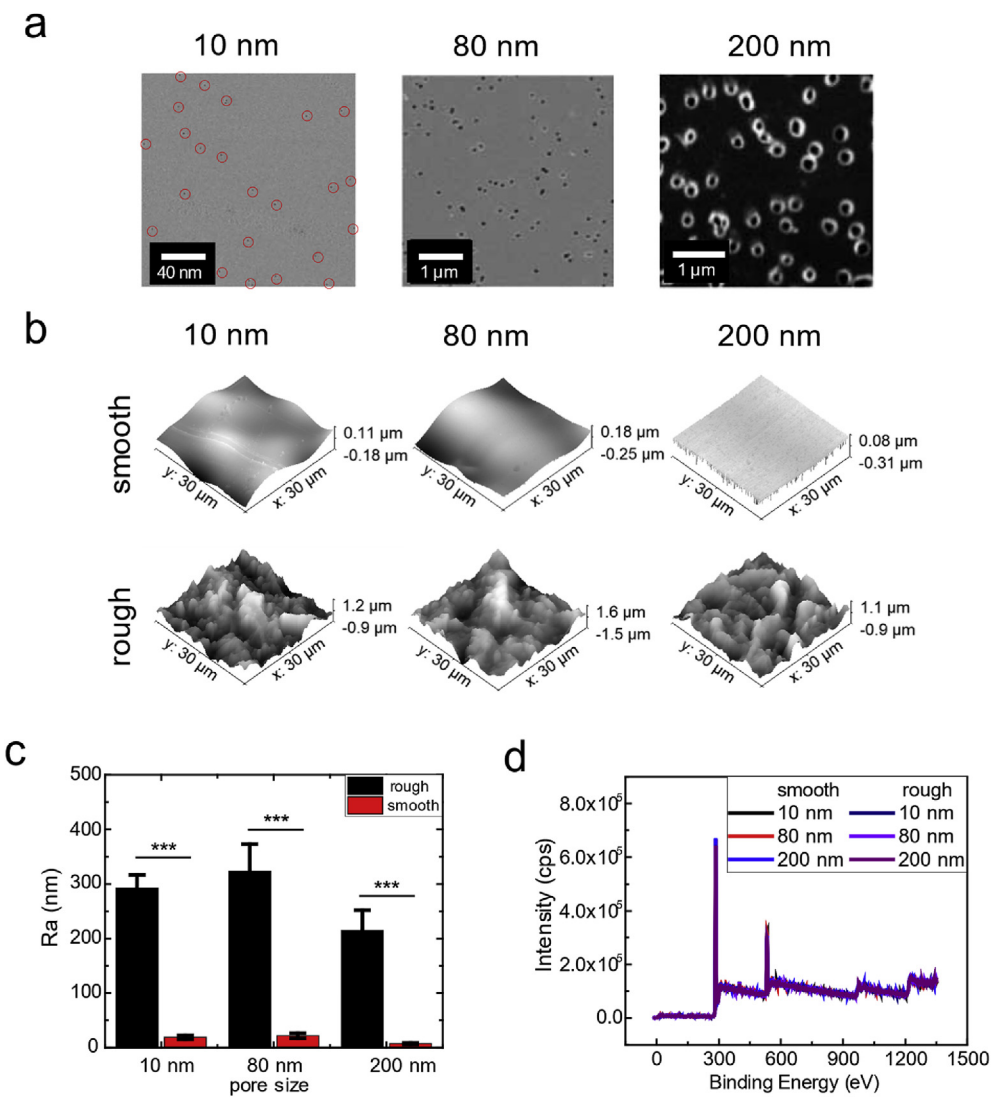

Fig. 1. Surface characterization of nanoporous membranes. (a) Representative scanning electron microscopy (SEM) images of smooth side of nanoporous polycarbonate membranes. Nanopore locations are marked out with red circles for 10 nm pore size membranes. (b) Representative 3D atomic force microscopy images of smooth (top row) and rough (bottom row) side of different pore size (10 nm, 80 nm, 200 nm) polycarbonate membranes. (c) Mean roughness (Ra) of the polycarbonate membrane surface based on AFM measurement (Mean ± Std, n = 3). (d) X-ray photoelectron spectroscopy (XPS) surface chemistry characterization of nanoporous polycarbonate membranes. (For interpretation of the references to colour in this figure legend, the reader is referred to the Web version of this article.)

temperature. Samples are then washed 5 times for 5 min each with PBS and incubated with goat anti mouse alexa 647 secondary antibodies (Thermo Fisher Scientific Inc, MA, USA) diluted 200X in 10% normal goat serum for 1 h in the dark. The cell nucleus is stained with DAPI. Stained cells are then washed 3 times for 5 min each with PBS and imaged with Axiozoom.V16 microscope (see Optical microscopic imaging).

For immunostaining of osteocalcin and osteopontin, cells are fixed after 24–26 days of culture in osteogenic differentiation medium. Briefly, cells are fixed with 4% formaldehyde and 0.1% Triton X100 diluted in PBS, followed by PBS wash for 3 times to remove excessive reagents. After fixation, cells are stained for osteocalcin and osteopontin. Fixed cells are blocked with 10% normal goat serum (Thermo Fisher Scientific Inc, MA, USA) in PBS for 1 h, followed by a two-step immunostaining process. Briefly, fixed cells are incubated with osteocalcin mouse monoclonal antibody (Santa Cruz Biotechnology, TX, USA) and osteopontin chicken polyclonal antibody (Thermo Fisher Scientific Inc, MA, USA) diluted 200 times in 10% normal goat serum for 1 h at room temperature. Samples are then washed 5 times for 5 min each with PBS and incubated with goat anti mouse alexa 647 secondary antibodies (Thermo Fisher Scientific Inc, MA, USA) and goat anti chicken alexa 488 secondary antibodies (Thermo Fisher Scientific Inc, MA, USA) diluted 200X in 10% normal goat serum for 1 h in the dark. Stained cells are then washed 3 times for 5 min each with PBS and imaged with Axiozoom.V16 microscope (see Optical microscopic imaging).

2.7. Optical microscopic imaging

For cell attachment, morphology, and focal adhesion assays, stained cells are observed using 25X/0.95-NA water immersion objective on a TCS-SP5 confocal laser scanning microscope (Leica Microsystems Inc., IL, USA). For cell attachment and focal adhesion studies, fluorescent images of the nucleus or focal adhesion in focus are taken. Image J is then used to analyze the number of nuclei or focal adhesion. For cell morphology studies, optical cross-sections are recorded at 0.3 μm z-axis interval to show intracellular fluorescence. Each slice image is taken at a scanning rate of 8000 Hz with line average of 2 to minimize photobleaching. Image J and MATLAB (Mathworks, MA, USA) with customized written code are used to analyze the images and calculate cell area, volume, and height. For cell differentiation assay, stained samples are fluorescently imaged using Plan-NEOFLUAR Z 1x objective on Axiozoom.V16 microscope (Carl Zeiss Microscopy, LLC, NY, USA). Fluorescence intensity of alkaline phosphatase protein, collagen, osteocalcin and osteopontin in each sample are measured by Image J.

2.8. Scanning electron microscopic imaging

For observation of cell morphology under the scanning electron microscope, fixed cell samples are dehydrated in ethanol graded series

(50%, 60%, 70%, 80%, 90%, 100%) for 30 min each and eventually immersed in 100% ethanol for 2 h. After dehydration, samples are transferred to a critical point dryer (Tousimis 931 GL, MD, USA) and dried under the critical point of CO_2. Samples are then coated with 5 nm Pt/PD and observed with Ultra 55 scanning electron microscope (Carl Zeiss Microscopy, LLC, NY, USA).

2.9. Statistical analysis

Statistical analysis is performed on Origin software. Statistical tests used one-way ANOVA for multiple comparisons, or Student's t-tests for comparison between two groups. P-values larger than 0.05 are assumed to be non-significant in all analyses; P-values smaller than 0.05 are marked with *; P-values lower than 0.01 are marked with **; P-values smaller than 0.001 are marked with ***.

3. Results

3.1. Nanoporous membrane characterization, and cell culture device fabrication

Nanoporous polycarbonate membranes are used as a model system to study effect of nanopore size and surface roughness on the BMSC behavior. We select commercially available nanoporous membranes which have randomly distributed nanopores that are mono-disperse in size due to the track etching method by which they are formed [24]. They also have different surface profile on each side, with one side rough and the other side smooth. During fabrication, these membranes are also treated with polyvinylpyrrolidone to make them hydrophilic, which enhances cell attachment [25]. We select membranes with different nanopore sizes (10 nm, 80 nm, 200 nm) to mimic the nanopore sizes found within cortical bone [20]. Membranes are examined by scanning electron microscopy (SEM), as shown in Fig. 1a. Additionally, SEM images of larger field of view are provided in Fig. S1. SEM images are further processed with Image J software to calculate the nanopore density of each membrane. Results confirm that membranes are of similar nanopore density, which are around 4×10^8 pores/cm^2, ensuring that the same number of nanopores is encountered by each cell. Furthermore, the open area (%) of the membrane is below 11%, suggesting majority of cell body is supported by the solid surface while it still interacts with the tiny nanopores on the surface, as shown in Table 1. Since the membranes have different roughness on each side, we characterize the topography of the two sides using AFM, as shown in Fig. 1b. The arithmetic average roughness (Ra) is calculated for the solid regions of nanoporous membranes. Results show that the roughness of one of the surfaces is an order of magnitude higher than the other surface, as shown in Fig. 1c; in this paper, we refer to them as rough and smooth, respectively. To confirm that the surface chemistry of the membranes is not affected by the porosity and roughness, X-ray photoelectron spectroscopy (XPS) analysis is performed on the various membranes. The XPS results show no difference among the chemical composition of membranes, as shown in Fig. 1d. Moreover, there are two peaks corresponding to carbon and oxygen with an area ratio of 3:1, as expected for polycarbonate. Furthermore, there is a small peak corresponding to nitrogen, which confirms the presence of a polyvinylpyrrolidone coating.

To culture cells, membranes are sandwiched between two spacer layers to ensure that the membrane is flat and that media can reach the cells from all sides. The sandwich structure is then UV sterilized, immersed in medium, and seeded with cells; a simplified workflow is shown in Fig. 2a. After 16 h, BMSC cells are examined under SEM after being fixed and dried using critical point drying. Images using an SEM suggest that cells are fully spread out and able to span over thousands of nanopores on the membranes, which shows that the membranes are biocompatible. Examples of BMSCs cultured on rough and smooth membranes with 80 nm pores are shown in Fig. 2b and c.

Table 1
Characterization of nanoporous membranes.

Nanopore size (nm)	10	80	200
Nanopore Density (pores/cm^2)	4.38×10^8	4.02×10^8	3.48×10^8
Open Area (%)	0.0344%	2.02%	10.91%

3.2. BMSC initial adhesion number on membranes

To investigate the effects of nanopore size and surface roughness on initial cell adhesion of BMSCs, we count the number of cells 16 h after seeding. For fluorescence imaging, we fix the cells and stain their nuclei using DAPI, as shown in Fig. 3a. Additionally, fluorescent images of larger field of view are provided in Fig. S2. Cell nuclei are then counted to determine the cell number. Surprisingly, our results show that porous membranes with larger nanopores have fewer cells attached, as shown in Fig. 3b. Since more hydrophilic surfaces can promote protein adsorption and thus enhance cell adhesion [25,26], we then quantify the hydrophilicity of the membranes by measuring static contact angle using sessile drop method. Indeed, membranes with larger nanopores have bigger contact angles, therefore, are less hydrophilic, as shown in Fig. S3. Meanwhile, as nanopore size increases from 10 nm to 200 nm, the solid surface area available for cell attachment decreases from 99.97% to 89.09% (Table 1), which may also contribute to decreased cell attachment. On membranes with larger nanopores, the decreased hydrophilicity and available surface area may inhibit cell adhesion, and thereby decrease cell adhesion number. While smooth surfaces reportedly encourage better attachment [12], we do not find that surface roughness significantly affects the initial cell adhesion number, as shown in Fig. 3b. This is different from other researches done on non-porous surface showing that better cell adhesion is achieved as roughness decrease from 105.6 nm to 1.8 nm[27]. We attribute our results to a larger contribution by nanopore size on cell adhesion, which overshadows the contribution by surface roughness, as surface discontinuity can greatly affect cell adhesion behavior[28], which is mainly determined by nanopore size in our scenario.

3.3. BMSC spreading behavior and focal adhesion size quantification

In addition, we also study the morphology of BMSC cells cultured on the membranes. We fluorescently stain the cell cytoplasm with cell tracker green and fix the cell with formaldehyde after 16 h of culture. Cells are then imaged by using confocal microscopy to obtain a z-stack images. The confocal images are further analyzed with MATLAB to calculate cell spreading area, volume and height. Top and side views of the 3D cell shape on smooth membranes are shown in Fig. 4a. Results show that the spreading area of BMSCs on the 200 nm pores is almost 2-fold larger than on 10 nm pores. By contrast, the spreading area increases only around 20% when the surface is smoother, as shown in Fig. 4b. Similarly, the volume of BMSCs on the 200 nm pores is almost 2-fold larger than on 10 nm pores, and a smooth surface results in a 25% increase in cell volume, as shown in Fig. 4c. The similar trends observed in cell spreading area and volume imply that the cell height is not affected by the different membrane conditions, as shown in Fig. S4.

Given that we see a dramatic change in spreading area, we hypothesize a corresponding change in focal adhesion structures, which are thought to involve in mechanotransduction process that can affect cell spreading area[29–31]. Focal adhesions (FA) are structures that mechanically link actin stress fibers, the force transducing unit during mechanotransduction, with the extracellular substrate through proteins such as vinculin [32–34]. A simplified schematic of cell adhesion structure is shown in Fig. 5a. To compare morphology of focal adhesions, we culture BMSCs on nanoporous membranes for 16 h and fluorescently stain actin and vinculin [35,36], followed by imaging

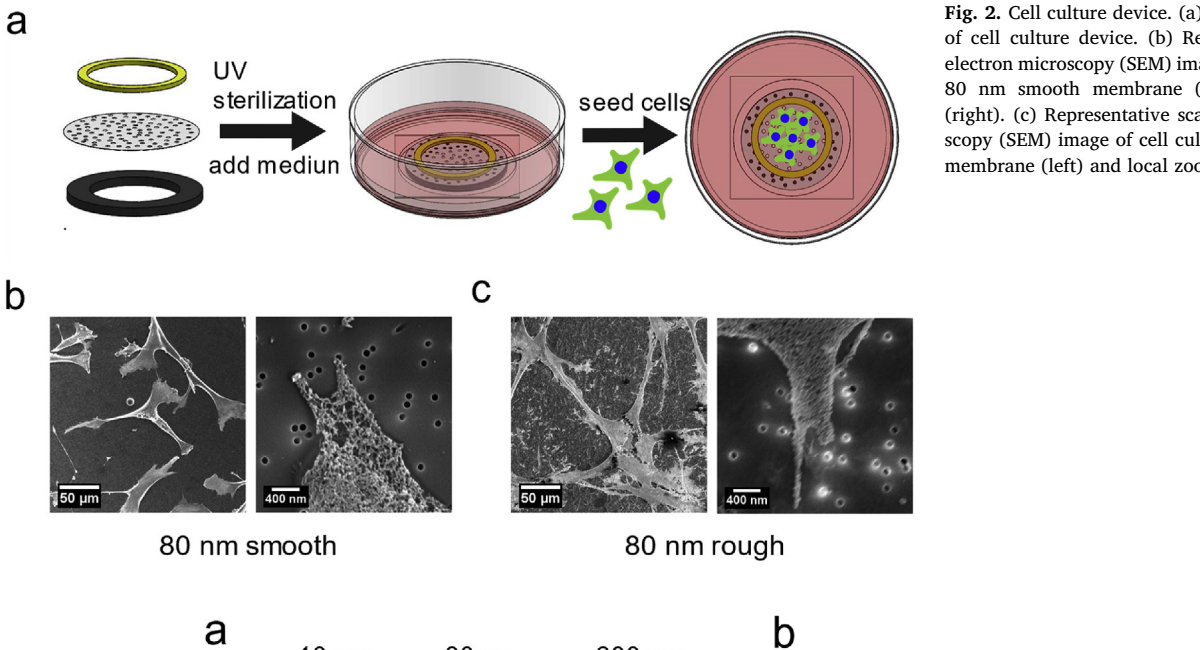

Fig. 2. Cell culture device. (a) Fabrication workflow of cell culture device. (b) Representative scanning electron microscopy (SEM) image of cells cultured on 80 nm smooth membrane (left) and local zoom (right). (c) Representative scanning electron microscopy (SEM) image of cell cultured on 80 nm rough membrane (left) and local zoom (right).

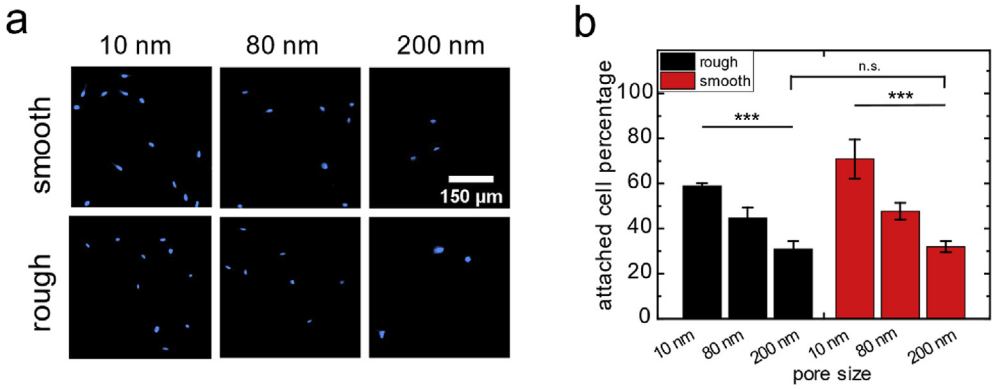

Fig. 3. Initial cell attachment percentage. (a) Nuclei stain of BMSC on smooth and rough side of membranes with different nanopore size, 16 h after seeding. (b) Initial cell attachment percentage after 16 h (Mean ± Std, n = 3).

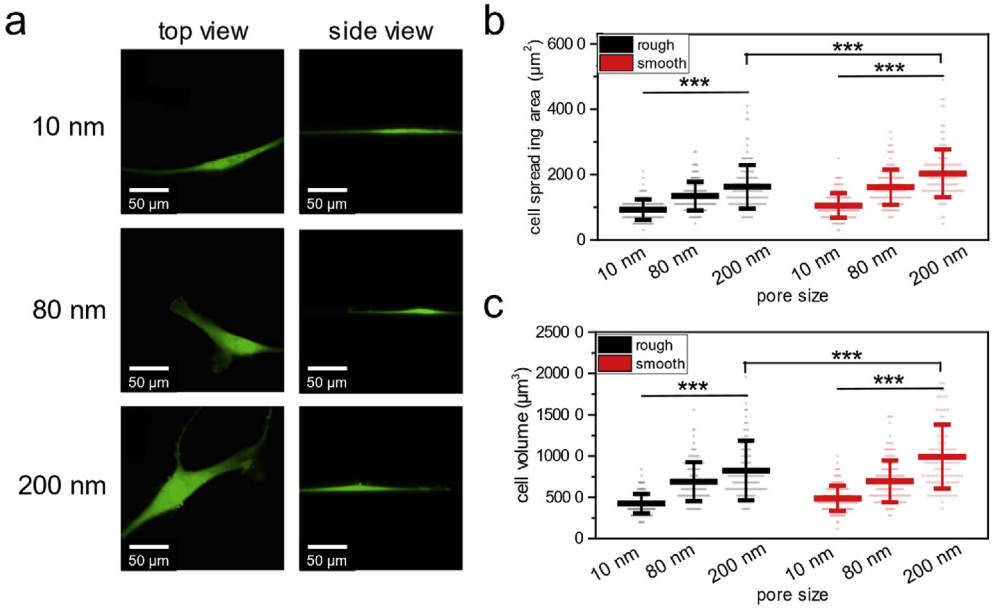

Fig. 4. Cell spreading behavior on nanoporous membranes. (a) Top and side view of confocal images of BMSC on smooth nanoporous membranes. (b) Cell spreading area on nanoporous membranes with different nanopore size and roughness (Mean ± Std, n > 100). (c) Cell volume on porous membranes with different nanopore size and roughness (Mean ± Std, n > 100).

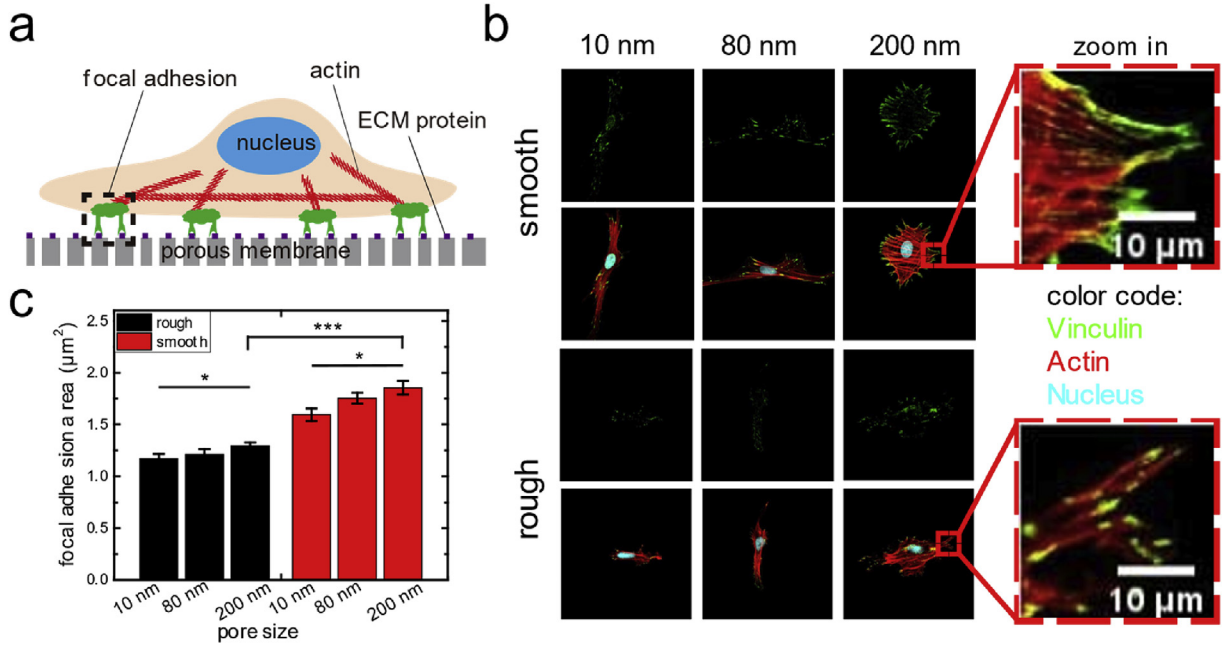

Fig. 5. Cell morphology and focal adhesion quantification. (a) Schematic cartoon of an adherent cell on nanoporous membranes. Cells adhere to ligands of extracellular matrix (ECM) on nanoporous membrane by focal adhesion, which is further connected by actin stress fiber inside cells. (b) Representative confocal microscope images of cells on different nanopore size and roughness membranes, vinculin (green), actin (red) and nucleus (cyan) are stained. (c) Individual focal adhesion area of cells on different nanopore size and roughness membrane (Mean ± Ste, n > 9, N > 700). (For interpretation of the references to colour in this figure legend, the reader is referred to the Web version of this article.)

them using confocal microscopy. Our results show that cells exhibit different cellular structures on membranes with different nanopore sizes when the roughness is held constant. When the nanopores are larger, cells are in spread-out, polygon shapes with thicker actin stress fibers, and focal adhesions are oval-shaped whose long axis is aligned with the actin stress fibers. The elongated FA shape indicates their maturation and suggests that strong adhesion is formed between cell and substrate [37,38]. On membranes with smaller nanopores, cells are elongated with fewer stress fibers and focal adhesions are round with no well-defined orientation, which suggests that focal adhesions are immature and that adhesion between the cells and substrate is poor, as shown in Fig. 5b. Interestingly, after quantifying the focal adhesion size, we find that the average focal adhesion size increases with nanopore size, as shown in Fig. 5c. Similarly, we find that surface roughness has a significant influence on focal adhesion morphology. On smooth surfaces, cells form large, oval focal adhesions, with orientations aligned with actin stress fibers, while on rough surfaces, focal adhesions are mostly small and round, as shown in Fig. 5b and c. Together, these results suggest both nanopore size and surface roughness play a significant role in regulating focal adhesion morphology and size, as larger nanopore and smoother surface promote larger focal adhesion formation, and at the same time, we see an increase of spreading area. This is consistent with previous reports showing a correlation between focal adhesion, morphology and cell spreading area[39].

In the nanopore sizes used, the total nanopore area ranges from less than 1% to over 10%, which may lead to differences in the diffusion of cell culture medium beneath the cells. To investigate whether the observed differences in cell spreading area are due to the diffusing profile difference as a result of different nanopore area, we fix the nanopore size of membranes at 200 nm and attach a polyacrylamide hydrogel layer underneath, which enables us to change the diffusion profile beneath the membrane without changing its surface topography, as illustrated in a simplified cartoon in Fig. S5a. The pore size of the gel is tuned by varying the acrylamide and N, N′-Methylenebisacrylamide concentration. As examined by scanning electron microcopy, the apparent pore radius of the dried gel sample change from 3 μm to 1.2 μm for acrylamide concentrations of 6%–12%, as shown in Fig. S5b. However, it's known that SEM will overestimate the pore size of hydrogel due to the drying process in the sample preparation. Standard procedures such as SDS-PAGE which use acrylamide concentration from 5% to 15% are able to size separate protein from ~212 kDa to ~13 kDa [40], which has the same size range as the protein in fetal bovine serum premixed in cell culture medium[40]. The hydrogel layer is therefore assumed to hinder the protein exchange between cell and culture medium beneath it. When BMSCs are cultured on the hydrogel-modified system, we find the presence of the hydrogel has no effect on cell spreading area or volume, as shown in Fig. S5c and Fig. S5d. These results suggest cell spreading area and volume are not influenced by the diffusion profile change beneath the membranes, suggesting membrane nanopore size might affect cell spreading area in the way by providing mechanical stimulus other than changing the diffusing profile.

3.4. Osteogenic differentiation of BMSC cells on nanoporous membranes

One of the primary functions of BMSC cells is their ability to differentiate into various lineages, of which osteogenic differentiation is most desirable for bone implant. Given that in short time scale, nanopore size and roughness can dramatically affect the cell attachment and spreading, we expect the long-term behavior of BMSC cells will also be altered. Since the membranes are very stiff (~Gpa), our system is particularly suitable to study osteogenic differentiation which is known to occur on stiff substrate [41,42]. In the process of osteogenic differentiation, ALP, an enzyme localized to the outside of the plasma membrane of cells, will be highly expressed in the early stage [43]. Then extracellular matrix proteins such as collagen type I, osteocalcin, and osteopontin will be secreted to initiate the mineralization process [44–47]. To induce differentiation, BMSC cells are seeded onto nanoporous membranes to grow in MSC growth media till confluency after 5–7 days, and subsequently cultured in osteogenic differentiation media. Then, to quantify the degree of osteogenic differentiation, we perform fluorescent staining on the four osteogenic marker proteins: Alkaline phosphotease protein (ALP), collagen type I, osteocalcin

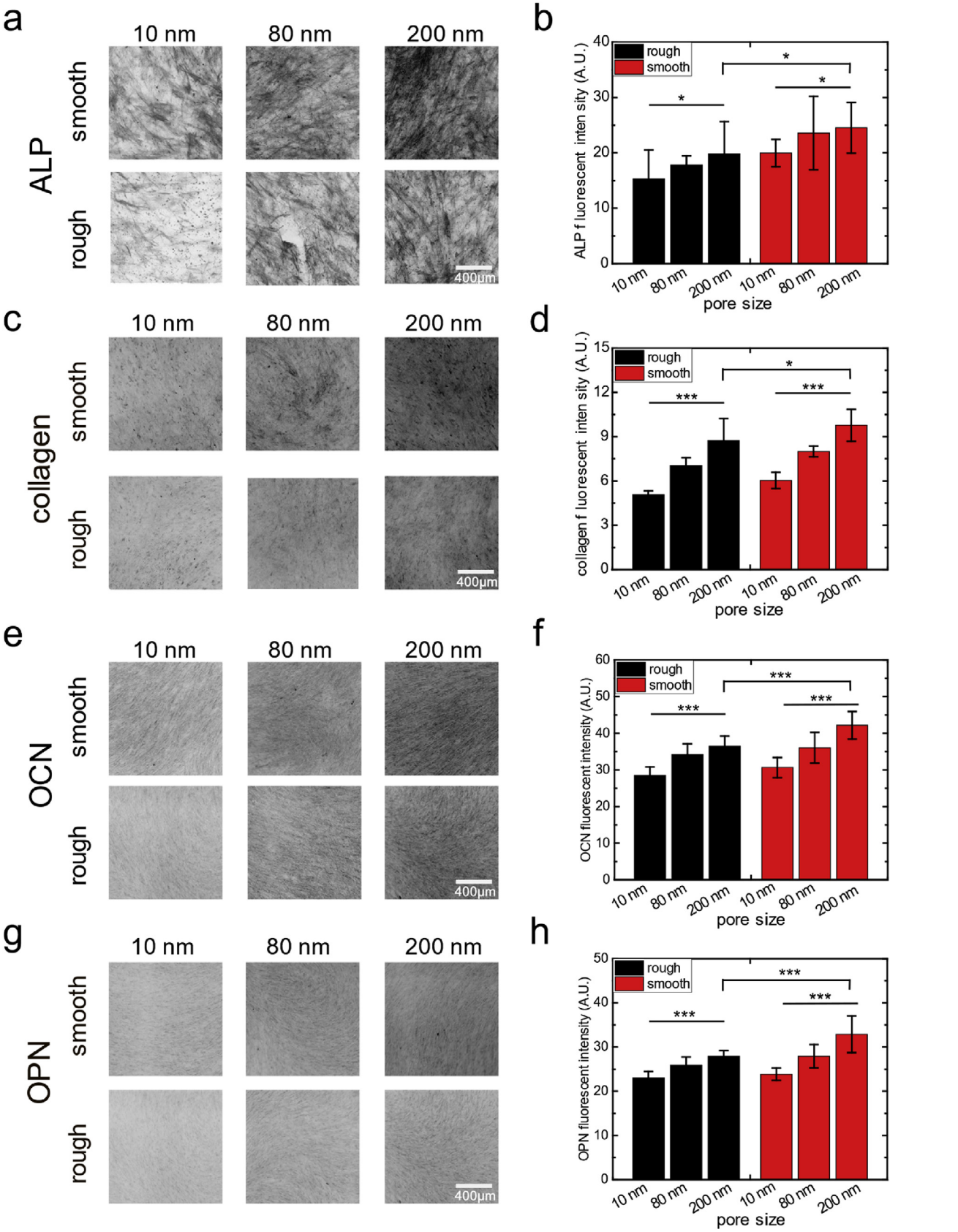

(caption on next page)

Fig. 6. BMSC differentiation on nanoporous membranes. (a) ALP fluorescent staining of BMSC monolayer after 16–18 days of culture in osteogenic differentiation media. (b) Fluorescence intensity quantification of ALP in BMSC monolayer (Mean ± Std, n = 3, N = 15). (c) Immunofluorescence staining of secreted collagen by BMSC monolayer after 16–18 days of culture in osteogenic differentiation media. (d) Fluorescence intensity quantification of immuno-stained collagen secreted by BMSC monolayer (Mean ± Std, n = 3, N = 15). (e) Immunofluorescence staining of secreted osteocalcin by BMSC monolayer after 24–26 days of culture in osteogenic differentiation media. (f) Fluorescence intensity quantification of immuno-stained osteocalcin secreted by BMSC monolayer (Mean ± Std, n = 3, N = 15). (g) Immunofluorescence staining of secreted osteopontin by BMSC monolayer after 24–26 days culture in osteogenic differentiation media. (h) Fluorescence intensity quantification of immuno-stained osteopontin secreted by BMSC monolayer (Mean ± Std, n = 3, N = 15).

(OCN), and osteopontin (OPN). ALP and collagen type I are stained after 16–18 days of culture in osteogenic differentiation media. Osteocalcin and osteopontin are stained after 24–26 days of culture in osteogenic differentiation media. ALP is fluorescently stained using ImmPACT® Vector® Red Alkaline Phosphatase (AP) Substrate and imaged under a fluorescence microscope, as shown in Fig. 6a. Other osteogenic differentiation markers, collagen type I, osteocalcin, and osteopontin are immunostained with fluorescent antibody and imaged with fluorescence microscope, results are shown in Fig. 6c, e, g. To compare ALP content between different samples, the average fluorescence intensity of each sample is calculated. Results show the fluorescence intensity of ALP is higher on membranes with larger nanopores, suggesting increase of nanopore size may stimulate the ALP expression, as shown in Fig. 6b. The bare membranes are used as negative control groups, which have fluorescence intensity 10-fold smaller than the cell samples, suggesting that the fluorescent signals in cell samples are mostly contributed by cell monolayer, but not membranes, as shown in Fig. S6a. By further measuring the ALP concentration in the culture media, we find that BMSC cells cultured on larger nanopore size also have higher ALP concentration, as shown in Fig. S7, which is consistent with the cell surface ALP measurement. Meanwhile, collagen type I secretion increases almost 2 times over the tested nanopore size range, as shown in Fig. 6d. Additionally, both osteocalcin and osteopontin increase almost 1.4 times over the tested nanopore size range, as shown in Fig. 6f, h. Moreover, the bare membranes are used as negative control groups, which have fluorescence intensity 10-fold smaller than the cell samples, suggesting the fluorescent signals in cell samples are mostly contributed by cell monolayer, but not membranes, as shown in Figs. S6b, c, d.

Since ALP, collagen type I, osteocalcin and osteopontin all increase with the nanopore size of the membranes, we conclude that increases of nanopore size can promote osteogenic differentiation of BMSC cells. Surface roughness, however, does not have a major influence on osteogenic differentiation, as suggested by minor change in fluorescence intensity of stained protein markers, though the change is still statistically significant, as shown in Fig. 6b, d, f, h. This suggests that nanopore size has a significant effect on the osteogenic differentiation of BMSC cells, whereas roughness only have a minor influence. Since nanopore size has significant effect on the short-time behavior of cell such as adhesion and spreading, which might eventually lead to the long-time behavior such as differentiation. These results suggest that initial cell adhesion number, cell spreading and osteogenic differentiation are all closely related.

4. Conclusions

In this study, we use nanoporous polycarbonate membranes to decouple the effects of nanopore size and roughness on BMSC cell adhesion, spreading and differentiation. We demonstrate that increasing nanopore size will inhibit the initial adhesion number of BMSC cells, but promote larger spreading area and cell volume. Furthermore, we find more osteogenic differentiation on larger nanopore size membranes, as indicated by higher expression levels of ALP, collagen type I, osteocalcin and osteopontin. In addition, changing the surface roughness does not have significant effect on initial adhesion of BMSC cells or their osteogenic differentiation, but instead, surface roughness plays a non-negligible role in regulating cell spreading area and volume. Overall, our results suggest that, both nanopore size and surface roughness can regulate the cell spreading and differentiation behavior, but to different extents; compared with surface roughness, nanopore size plays a more significant role in governing BMSC cell behavior. Not only does nanopore size affects the short-time behavior such as adhesion and spreading, but also affects the long-time behavior such as differentiation, which suggests that nanopore size affect long-time behavior by affecting short-time behavior. This is supported by other studies using different substrate system such as petridish and PDMS, which shows that increased spreading area or decreased initial cell plating density can promote BMSC osteogenic differentiation [48–50]. Surprisingly, our results find similar behavior even though our membrane material is markedly different from other substrate system, suggesting that the regulation of BMSC differentiation by mechanical signals happens by a mechanism that is intrinsic to the cells. These results suggest that initial cell adhesion number, cell spreading and osteogenic differentiation are all closely related. However, the biological mechanism to connect these behaviors is not clear and deserves more study.

CRediT authorship contribution statement

Jing Xia: Investigation, Formal analysis, Conceptualization, Writing - original draft, Writing - review & editing. **Yuan Yuan:** Investigation, Formal analysis. **Huayin Wu:** Writing - review & editing. **Yuting Huang:** Writing - review & editing. **David A. Weitz:** Conceptualization, Funding acquisition, Supervision, Writing - review & editing.

Declaration of competing interest

The authors declare that they have no known competing financial interests or personal relationships that could have appeared to influence the work reported in this paper.

Acknowledgement

We thank David J. Mooney (Harvard University) for helpful discussions and suggestions. This work was supported by the National Science Foundation (DMR-1708729), the Harvard Materials Research Science and Engineering Center (DMR-1420570), and the National Institutes of Health, United States (EB023287). The authors confirm that there are no known conflicts of interest associated with this publication and there has been no significant financial support for this work that could have influenced its outcome.

Appendix A. Supplementary data

Supplementary data to this article can be found online at https://doi.org/10.1016/j.biomaterials.2020.120014.

References

[1] A. Augello, C. De Bari, The regulation of differentiation in mesenchymal stem cells, Hum. Gene Ther. 21 (10) (2010) 1226–1238.
[2] A. Muraglia, R. Cancedda, R. Quarto, Clonal mesenchymal progenitors from human bone marrow differentiate in vitro according to a hierarchical model, J. Cell Sci. 113 (7) (2000) 1161–1166.
[3] T. Yoshiya, N. Shingo, O. Yosuke, Osteoblasts and osteoclasts in bone remodeling and inflammation, Curr. Drug Targets - Inflamm. Allergy 4 (3) (2005) 325–328.

[4] J.C. Crockett, M.J. Rogers, F.P. Coxon, L.J. Hocking, M.H. Helfrich, Bone remodelling at a glance, J. Cell Sci. 124 (7) (2011) 991.
[5] E.M. Horwitz, D.J. Prockop, L.A. Fitzpatrick, W.W.K. Koo, P.L. Gordon, M. Neel, M. Sussman, P. Orchard, J.C. Marx, R.E. Pyeritz, M.K. Brenner, Transplantability and therapeutic effects of bone marrow-derived mesenchymal cells in children with osteogenesis imperfecta, Nat. Med. 5 (1999) 309.
[6] A.I. Caplan, S.P. Bruder, Mesenchymal stem cells: building blocks for molecular medicine in the 21st century, Trends Mol. Med. 7 (6) (2001) 259–264.
[7] A. Freidenstein, Osteogenic Stem Cells in Bone Marrow, Bone and mineral research, 1990, pp. 243–272.
[8] P. Bianco, M. Riminucci, S. Gronthos, P.G. Robey, Bone marrow stromal stem cells: nature, biology, and potential applications, Stem Cell. 19 (3) (2001) 180–192.
[9] J. Zhao, C. Yang, C. Su, M. Yu, X. Zhang, S. Huang, G. Li, M. Yu, X. Li, Reconstruction of orbital defects by implantation of antigen-free bovine cancellous bone scaffold combined with bone marrow mesenchymal stem cells in rats, Graefe's Arch. Clin. Exp. Ophthalmol. 251 (5) (2013) 1325–1333.
[10] A. Klymov, L. Prodanov, E. Lamers, J.A. Jansen, X.F. Walboomers, Understanding the role of nano-topography on the surface of a bone-implant, Biomater. Sci. 1 (2) (2013) 135–151.
[11] N. Khosravi, A. Maeda, R.S. DaCosta, J.E. Davies, Nanosurfaces modulate the mechanism of peri-implant endosseous healing by regulating neovascular morphogenesis, Commun. Biol. 1 (1) (2018) 1–13.
[12] W. Chen, Y. Shao, X. Li, G. Zhao, J. Fu, Nanotopographical surfaces for stem cell fate control: Engineering mechanobiology from the bottom, Nano Today 9 (6) (2014) 759–784.
[13] N. Reznikov, M. Bilton, L. Lari, M.M. Stevens, R. Kröger, Fractal-like hierarchical organization of bone begins at the nanoscale, Science 360 (6388) (2018).
[14] S. Pujari-Palmer, T. Lind, W. Xia, L. Tang, M. Karlsson Ott, Controlling osteogenic differentiation through nanoporous alumina, J. Biomaterials Nanobiotechnol. (2014) 98–104 05(02).
[15] S. Oh, K.S. Brammer, Y.S. Li, D. Teng, A.J. Engler, S. Chien, S. Jin, Stem cell fate dictated solely by altered nanotube dimension, Proc. Natl. Acad. Sci. U. S. A. 106 (7) (2009) 2130–2135.
[16] J. Park, S. Bauer, K. von der Mark, P. Schmuki, Nanosize and Vitality: TiO2 nanotube diameter directs cell fate, Nano Lett. 7 (6) (2007) 1686–1691.
[17] A.A. Khalili, M.R. Ahmad, A review of cell adhesion studies for biomedical and biological applications, Int. J. Mol. Sci. 16 (8) (2015) 18149–18184.
[18] J.L. McGrath, Cell spreading: the power to simplify, Curr. Biol. 17 (10) (2007) R357–R358.
[19] J.A. Burdick, G. Vunjak-Novakovic, Engineered microenvironments for controlled stem cell differentiation, Tissue Eng. 15 (2) (2008) 205–219.
[20] P. Milovanovic, Z. Vukovic, D. Antonijevic, D. Djonic, V. Zivkovic, S. Nikolic, M. Djuric, Porotic paradox: distribution of cortical bone pore sizes at nano-and micro-levels in healthy vs. fragile human bone, J. Mater. Sci. Mater. Med. 28 (5) (2017) 71.
[21] P. Milovanovic, M. Djuric, O. Neskovic, D. Djonic, J. Potocnik, S. Nikolic, M. Stoiljkovic, V. Zivkovic, Z. Rakocevic, Atomic force microscopy characterization of the external cortical bone surface in young and elderly women: potential nanostructural traces of periosteal bone apposition during aging, Microsc. Microanal. 19 (5) (2013) 1341–1349.
[22] D. Deligianni, Effect of surface roughness of the titanium alloy Ti–6Al–4V on human bone marrow cell response and on protein adsorption, Biomaterials 22 (11) (2001) 1241–1251.
[23] K.E. Smith, S.L. Hyzy, M. Sunwoo, K.A. Gall, Z. Schwartz, B.D. Boyan, The dependence of MG63 osteoblast responses to (meth)acrylate-based networks on chemical structure and stiffness, Biomaterials 31 (24) (2010) 6131–6141.
[24] B.A. Sartowska, Nanopores with controlled profiles in track-etched membranes, Nukleonika 57 (4) (2012) 575–579.
[25] L. Jin Ho, L. Sang Jin, G. Khang, L. Hai Bang, Interaction of fibroblasts on polycarbonate membrane surfaces with different micropore sizes and hydrophilicity, J. Biomater. Sci. Polym. Ed. 10 (3) (1999) 283–294.
[26] L. Hao, H. Yang, C. Du, X. Fu, N. Zhao, S. Xu, F. Cui, C. Mao, Y. Wang, Directing the fate of human and mouse mesenchymal stem cells by hydroxyl-methyl mixed self-assembled monolayers with varying wettability, J. Mater. Chem. B 2 (30) (2014) 4794–4801.
[27] S. Migita, K. Araki, Effect of nanometer scale surface roughness of titanium for osteoblast function, AIMS Bioeng. 4 (1) (2016) 162–170.
[28] E. Babaliari, P. Kavatzikidou, D. Angelaki, L. Chaniotaki, A. Manousaki, A. Siakouli-Galanopoulou, A. Ranella, E. Stratakis, Engineering cell adhesion and orientation via ultrafast laser fabricated microstructured substrates, Int. J. Mol. Sci. 19 (7) (2018) 2053.
[29] J. Han Sangyoon, Kevin S. Bielawski, H. Ting Lucas, Marita L. Rodriguez, Nathan J. Sniadecki, Decoupling substrate stiffness, spread area, and micropost density: a close spatial relationship between traction forces and focal adhesions, Biophys. J. 103 (4) (2012) 640–648.
[30] C.W. Kuo, D.-Y. Chueh, P. Chen, Investigation of size–dependent cell adhesion on nanostructured interfaces, J. Nanobiotechnol. 12 (1) (2014) 54.
[31] D.-H. Kim, D. Wirtz, Predicting how cells spread and migrate: focal adhesion size does matter, Cell Adhes. Migrat. 7 (3) (2013) 293–296.
[32] R. Dominguez, K.C. Holmes, Actin structure and function, Annu. Rev. Biophys. 40 (1) (2011) 169–186.
[33] T.D. Pollard, J.A. Cooper, Actin, a central player in cell shape and movement, Science 326 (5957) (2009) 1208.
[34] K. Hayakawa, H. Tatsumi, M. Sokabe, Mechano-sensing by actin filaments and focal adhesion proteins, Commun. Integr. Biol. 5 (6) (2012) 572–577.
[35] G.R. Owen, D. Meredith, R. Richards, Focal adhesion quantification-a new assay of material biocompatibility? Review, Eur. Cell. Mater. 9 (2005) 85–96 discussion 85-96.
[36] U. Horzum, B. Ozdil, D. Pesen-Okvur, Step-by-step quantitative analysis of focal adhesions, MethodsX 1 (2014) 56–59.
[37] B. Geiger, A. Bershadsky, R. Pankov, K.M. Yamada, Transmembrane crosstalk between the extracellular matrix and the cytoskeleton, Nat. Rev. Mol. Cell Biol. 2 (2001) 793.
[38] P.T. Ohara, R.C. Buck, Contact guidance in vitro: a light, transmission, and scanning electron microscopic study, Exp. Cell Res. 121 (2) (1979) 235–249.
[39] C.W. Kuo, D.-Y. Chueh, P. Chen, Investigation of size-dependent cell adhesion on nanostructured interfaces, J. Nanobiotechnol. 12 (2014) 54-54.
[40] N. Miękus, I. Olędzka, A. Plenis, Z. Woźniak, A. Lewczuk, P. Koszałka, B. Seroczyńska, T. Bączek, Gel electrophoretic separation of proteins from cultured neuroendocrine tumor cell lines, Mol. Med. Rep. 11 (2) (2015) 1407–1415.
[41] A.J. Engler, S. Sen, H.L. Sweeney, D.E. Discher, Matrix elasticity directs stem cell lineage specification, Cell 126 (4) (2006) 677–689.
[42] R. Olivares-Navarrete, E.M. Lee, K. Smith, S.L. Hyzy, M. Doroudi, J.K. Williams, K. Gall, B.D. Boyan, Z. Schwartz, Substrate stiffness controls osteoblastic and chondrocytic differentiation of mesenchymal stem cells without exogenous stimuli, PloS One 12 (1) (2017) e0170312-e0170312.
[43] R. Marom, I. Shur, R. Solomon, D. Benayahu, Characterization of adhesion and differentiation markers of osteogenic marrow stromal cells, J. Cell. Physiol. 202 (1) (2005) 41–48.
[44] Z. Huang, E.R. Nelson, R.L. Smith, S.B. Goodman, The sequential expression profiles of growth factors from osteoprogenitors [correction of osteroprogenitors] to osteoblasts in vitro, Tissue Eng. 13 (9) (2007) 2311–2320.
[45] Q.L. Darryl, Y.D.A., L.L.W., C. RashmiW.R.J., Distinct proliferative and differentiated stages of murine MC3T3-E1 cells in culture: an in vitro model of osteoblast development, J. Bone Miner. Res. 7 (6) (1992) 683–692.
[46] E.M. Aarden, A.M.M. Wassenaar, M.J. Alblas, P.J. Nijweide, Immunocytochemical demonstration of extracellular matrix proteins in isolated osteocytes, Histochem. Cell Biol. 106 (5) (1996) 495–501.
[47] R. Miron, Y. Zhang, Osteoinduction: a review of old concepts with new standards, J. Dent. Res. 91 (8) (2012) 736–744.
[48] R. McBeath, D.M. Pirone, C.M. Nelson, K. Bhadriraju, C.S. Chen, Cell shape, cytoskeletal tension, and RhoA regulate stem cell lineage commitment, Dev. Cell 6 (4) (2004) 483–495.
[49] M.F. Pittenger, A.M. Mackay, S.C. Beck, R.K. Jaiswal, R. Douglas, J.D. Mosca, M.A. Moorman, D.W. Simonetti, S. Craig, D.R. Marshak, Multilineage potential of adult human mesenchymal stem cells, Science 284 (5411) (1999) 143–147.
[50] K.A. Kilian, B. Bugarija, B.T. Lahn, M. Mrksich, Geometric cues for directing the differentiation of mesenchymal stem cells, Proc. Natl. Acad. Sci. U. S. A. 107 (11) (2010) 4872–4877.